Cell

Kinetochore Microtubule Dynamics and Attachment Stability Are Regulated by Hec1

Jennifer G. DeLuca,[1,4,*] Walter E. Gall,[1,4] Claudio Ciferri,[3] Daniela Cimini,[2] Andrea Musacchio,[3] and E.D. Salmon[1]
[1] Department of Biology, University of North Carolina at Chapel Hill, Chapel Hill, NC 27599, USA
[2] Department of Biological Sciences, Virginia Polytechnic Institute and State University, Blacksburg, VA 24061, USA
[3] Department of Experimental Oncology, European Institute of Oncology, Via Ripamonti 435, 20141 Milan, Italy
[4] These authors contributed equally to this work.
*Contact: jgdeluca@email.unc.edu
DOI 10.1016/j.cell.2006.09.047

SUMMARY

Mitotic cells face the challenging tasks of linking kinetochores to growing and shortening microtubules and actively regulating these dynamic attachments to produce accurate chromosome segregation. We report here that Ndc80/Hec1 functions in regulating kinetochore microtubule plus-end dynamics and attachment stability. Microinjection of an antibody to the N terminus of Hec1 suppresses both microtubule detachment and microtubule plus-end polymerization and depolymerization at kinetochores of PtK1 cells. Centromeres become hyperstretched, kinetochore fibers shorten from spindle poles, kinetochore microtubule attachment errors increase, and chromosomes severely mis-segregate. The N terminus of Hec1 is phosphorylated by Aurora B kinase in vitro, and cells expressing N-terminal nonphosphorylatable mutants of Hec1 exhibit an increase in merotelic attachments, hyperstretching of centromeres, and errors in chromosome segregation. These findings reveal a key role for the Hec1 N terminus in controlling dynamic behavior of kinetochore microtubules.

INTRODUCTION

The goal of mitosis is to properly segregate a replicated set of chromosomes into two daughter cells. The mitotic spindle, which is comprised of an elaborate set of microtubules (MTs) and microtubule-associated proteins (MAPs), is largely responsible for executing this task. Spindle MTs attach to a specialized protein region on the chromosomes called the kinetochore, and it is through this interaction that force is generated for chromosome movements during mitosis. MTs are highly dynamic polymers that switch between states of polymerization and depolymerization at their plus ends. To maintain connection with the mitotic spindle, kinetochores must hold on to MT plus ends as they exhibit this dynamic behavior. Kinetochores must also release the plus ends of MTs attached to the wrong spindle pole to ensure proper chromosome bi-orientation. Thus, two key aspects of kinetochore microtubules (kMTs) must be actively regulated: (1) attachment stability within kinetochore-binding sites and (2) plus-end assembly dynamics. We are just beginning to understand how the kinetochore accomplishes these tasks, and central to the problem is the Ndc80 complex of proteins.

The Ndc80 complex is comprised of Ndc80 (Hec1 in humans for *H*ighly *E*xpressed in *C*ancer, Chen et al., 1997), Nuf2, Spc24, and Spc25. Studies in budding yeast, followed by studies in many other eukaryotic systems, have demonstrated that the Ndc80 complex is required for robust kMT attachments (reviewed in Maiato et al., 2004). The Ndc80 complex is approximately 50 nm long and is dumb-bell shaped, with the globular N-terminal heads of Hec1 and Nuf2 at one end and the globular C-terminal heads of Spc24 and Spc25 at the opposite end of a central rod domain (Wei et al., 2005; Ciferri et al., 2005). Hec1 has recently been localized by immunoelectron microscopy (EM) to the outer plate of the vertebrate kinetochore (DeLuca et al., 2005), the region of the kinetochore where MT plus ends terminate and polymerization/depolymerization occurs. The mechanism by which this complex contributes to kMT attachment remains unknown. In budding yeast, the MT-binding Dam1 complex has been implicated in mediating kMT attachment (Cheeseman et al., 2001, 2002), perhaps by forming a ring of subunits around MT plus ends (Miranda et al., 2005; Westermann et al., 2005).

The Ndc80 complex may also have a key role in preventing chromosome missegregation by releasing improperly attached MTs from kinetochores. Merotelic kinetochore attachment (in which a kinetochore is attached to MTs emanating from both spindle poles) is a major cause of anaphase lagging chromosomes and

aneuploidy in mammalian tissue cells (Cimini et al., 2001). Budding yeast Ipl1p kinase plays a role in destabilizing kMT attachments (Tanaka et al., 2002; Cheeseman et al., 2002; Pinsky et al., 2006), and it has been suggested, but not demonstrated, that regulation of destabilization occurs through Dam1 and Ndc80 (Shang et al., 2003). Aurora B kinase is a homolog of Ipl1p in vertebrate cells that is needed for proper chromosome segregation and kinetochore function. This conserved kinase likely has multiple protein targets at kinetochores (Cheeseman et al., 2002; Tien et al., 2004; Nousiainen et al., 2006). Partial inhibition of Aurora B kinase activity enhances kMT stability (Hauf et al., 2003; Cimini et al., 2006). Strong kinase inhibition or Aurora B protein depletion results in a failure to build kinetochores capable of properly attaching to MTs and achieving bi-orientation on the mitotic spindle (reviewed in Carmena and Earnshaw, 2003).

We report here that the N terminus of Hec1 has key functions in regulating both plus-end attachment stability and plus-end assembly dynamics of kMTs, and these functions depend, in part, on phosphorylation by Aurora B kinase.

RESULTS

Antibody 9G3 Binds the N Terminus of Hec1, Exterior to Spc24 at Metaphase Kinetochores

We mapped the epitope on Hec1 recognized by 9G3, a monoclonal antibody originally raised to a large portion of recombinantly expressed human Hec1 (amino acids 56–642; Chen et al., 1997). An overlapping peptide array covering the entire amino acid sequence of Hec1 was generated and subjected to an immuno-dot blot, using 9G3 as a probe. The antibody recognized one peptide (C-2), which corresponded to amino acids 200–215 (Figure 1A) of the N-terminal globular domain of Hec1 (Figure 1B; Wei et al., 2005; Ciferri et al., 2005). The binding of 9G3 to peptide C-2 was specific, as preincubation of the peptide with 9G3 prevented the antibody from recognizing kinetochores in immunofluorescence assays (Figure S1 available with this article online).

We coimmunostained HeLa and PtK1 cells in metaphase with 9G3 and an antibody to Spc24 (McCleland et al., 2004). The N terminus of Hec1 was always exterior to Spc24 at kinetochores of bi-oriented chromosomes (Figures 1C and 1D). Antibody 9G3 was previously used to localize Hec1 to the kinetochore outer plate by immuno-EM (DeLuca et al., 2005). Thus, the Ndc80 complex is oriented with the N-terminal globular domains of Hec1 and Nuf2 proximal to the plus ends of kMTs within the outer plate and the Spc24 and Spc25 end of the complex closer to the inner kinetochore on bi-oriented chromosomes at metaphase.

PtK1 Cells Exhibit Mitotic Defects following 9G3 Injection

To test the function of the Hec1 N-terminal globular domain, we microinjected 9G3 into mitotic PtK1 cells. Antibody 9G3 recognized one major band at ~75 kDa from PtK1 extracts, consistent with the predicted molecular weight of Hec1 (Chen et al., 1997; Figure 1E). Injected 9G3 concentrated at kinetochores, distal from the inner kinetochore proteins recognized by the CREST serum, and did not strongly label spindle MTs or spindle poles (Figure 1F). Spc24 remained localized to kinetochores (data not shown), indicating that the Ndc80 complex was intact and able to bind kinetochores after 9G3 injection.

Chromosome movements of injected cells were followed by phase-contrast timelapse microscopy (Figure 2A). Prophase cells injected with 9G3 entered anaphase 52 ± 14 min after nuclear envelope breakdown (n = 35), compared to 29 ± 4 min for buffer-injected cells (n = 16). Thus, 9G3 injection resulted in a slight, but statistically significant delay in anaphase onset (t test p value < 0.001). Cells injected with 9G3 retained a functional Mad2-dependent spindle assembly checkpoint, as they localized high levels of Mad2 to unattached kinetochores, lost Mad2 as chromosomes became bi-oriented, and entered anaphase with Mad2-depleted kinetochores in a manner similar to control cells (Figure S2; Howell et al., 2000).

Unlike control cells, however, 9G3-injected prophase or prometaphase cells were unable to properly align their chromosomes and experienced severe defects in anaphase chromosome segregation. Of 17 cells injected in prophase or prometaphase, all 17 entered anaphase with unaligned chromosomes (Figures 2A and 2B). In addition, 15 of 17 cells injected with 9G3 in prophase or prometaphase had at least one lagging chromosome in anaphase (Figure 2A, arrows). When injected into metaphase cells, 9G3 did not induce chromosomes to leave the metaphase plate but increased the frequency of lagging chromosomes in anaphase (Figures 2A and 2B). In contrast, no cells injected with injection buffer alone (n = 22) or a nonperturbing antibody to the kinetochore protein CENP-F (Cimini et al., 2004) (n = 10) entered anaphase with unaligned chromosomes or exhibited lagging chromosomes in anaphase. Our live-cell imaging results are consistent with previously published experiments describing 9G3 injection into S phase T24 human bladder carcinoma cells, in which injected cells failed to form coherent metaphase plates and entered anaphase with unaligned chromosomes (Chen et al., 1997).

Robust but Erroneous kMT Attachment Occurs after 9G3 Injection

All kinetochores on chromosomes in 9G3-injected cells that had progressed to late prometaphase or further had robust kinetochore fibers (Figure 3A). These fibers persisted after a cold/calcium treatment (Brinkley and Cartwright, 1975; Weisenberg and Deery, 1981), demonstrating they were bona fide kMTs (Figure 3B). The kinesin-7 protein, CENP-E, assists in recruiting MTs to the kinetochore and in spindle checkpoint inactivation (Mao et al., 2003). Consistent with our observation that 9G3-injected cells form robust kMT attachments, CENP-E protein levels

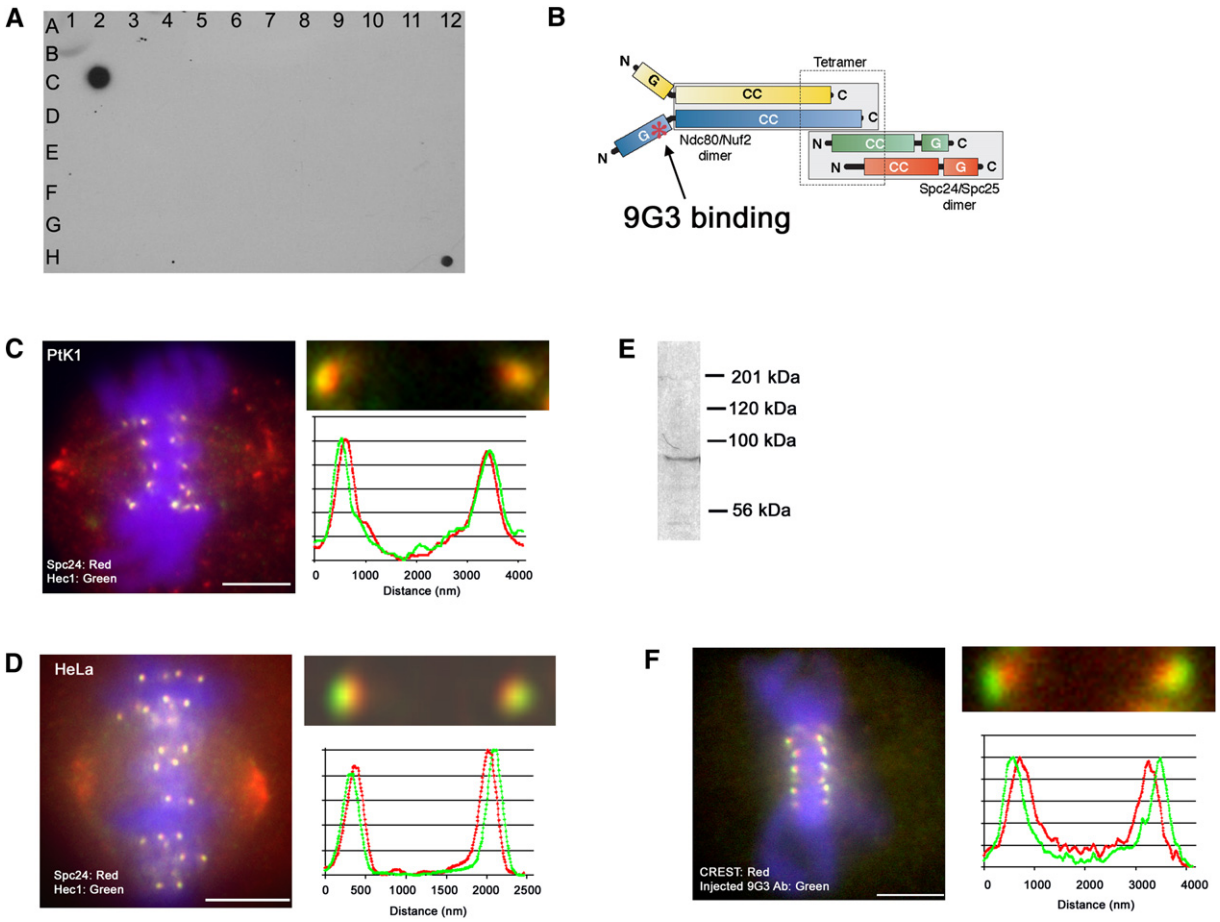

Figure 1. Epitope Mapping and Cellular Localization of Hec1 Monoclonal Antibody 9G3

(A) Peptides covering the sequence of human Hec1 were adsorbed onto nitrocellulose and immunoprobed with 9G3. As a control, HeLa extract was adsorbed onto the nitrocellulose at region H-12. Both the control spot and spot C-2 (amino acids 200–215) were positively identified.

(B) Representation of the Ndc80 complex as predicted from previous publications (Wei et al., 2005; Ciferri et al., 2005). The asterisk marks the site on Hec1 where 9G3 binds.

(C and D) Localization of 9G3 (green) and an antibody to Spc24 (red) in PtK1 cells (C) and HeLa cells (D). Linescans were carried out on sister kinetochore pairs from both HeLa cells (n = 40 pairs/3 cells) and PtK1 cells (n = 34 pairs/4 cells), and in all cases Hec1 localized exteriorly to Spc24 at kinetochores.

(E) Western blot of whole-cell PtK1 extract with 9G3 as a probe.

(F) Immunofluorescent image of a PtK1 cell injected with 9G3. To the right of each cell panel in (C), (D), and (F), a single kinetochore pair has been enlarged. The graphs represent the linescan data from the single kinetochore pair. Scale bars in (C), (D), and (F) = 5 μm.

at kinetochores were not reduced from control levels (Figure S3).

Analysis of 9G3-injected cells immunostained with tubulin antibodies revealed a high frequency of merotelic kinetochores (Figure 3A). Seventy-six percent of injected cells had at least one merotelically oriented kinetochore, and 56% had multiple merotelic kinetochores (n = 89 cells). In contrast, merotelic kinetochores are less frequent in control cells: 30% of control prometaphase PtK1 cells and 16.3% of control metaphase PtK1 cells exhibit one merotelically attached kinetochore (Cimini et al., 2003), and only 2% of control late prometaphase and metaphase PtK1 cells contain multiple merotelic attachments (Cimini et al., 2006).

9G3 Injection Results in Hyperstretched Kinetochores and Shortened Kinetochore Fibers

To determine if the robust kinetochore fibers observed in 9G3-injected cells were able to generate tension, we measured interkinetochore distances between sister kinetochores of bi-oriented chromosomes (Figure 3C). Surprisingly, the average distance in 9G3-injected cells was 1.5× greater than that for uninjected cells (Figure 3E; t test p value < 0.001). This effect was dependent on MT attachment, as the average value for interkinetochore distance in 9G3-injected prophase cells was identical to values from uninjected prophase cells (Figure 3E) and uninjected cells treated with 10 μM nocodazole to depolymerize all MTs (data not shown).

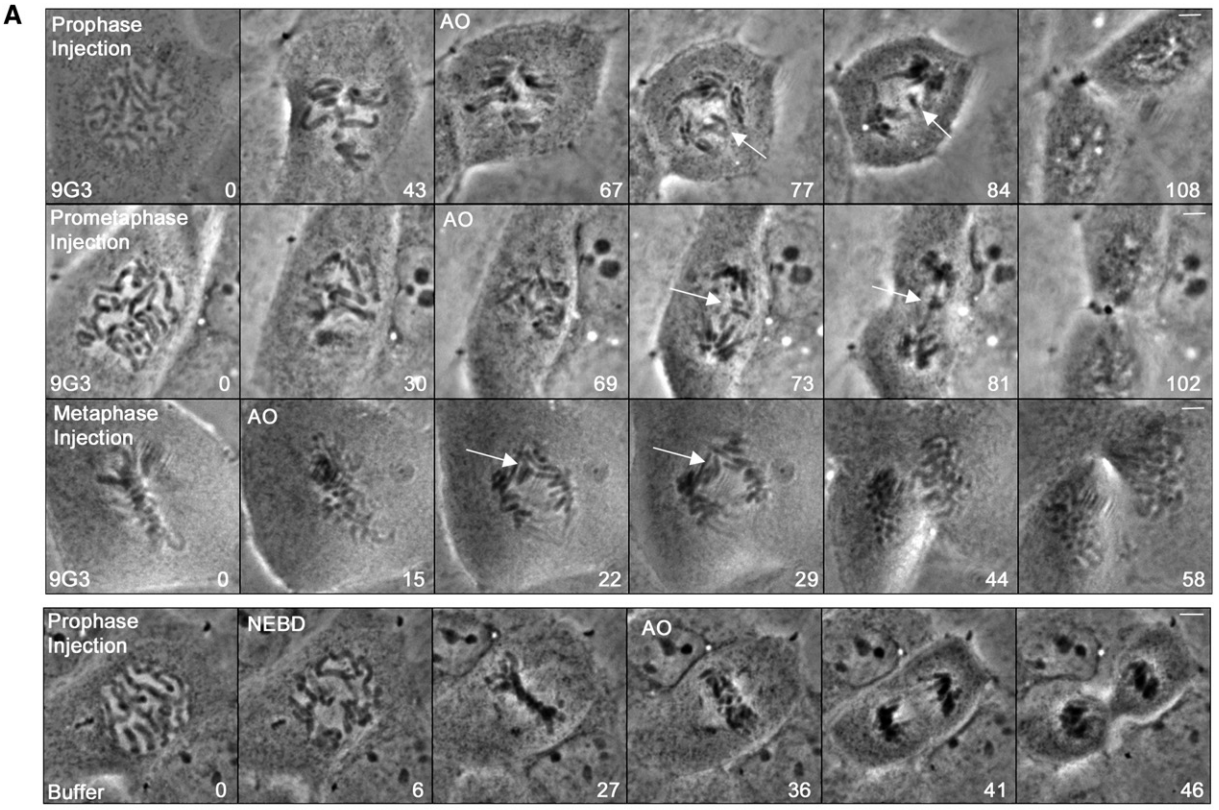

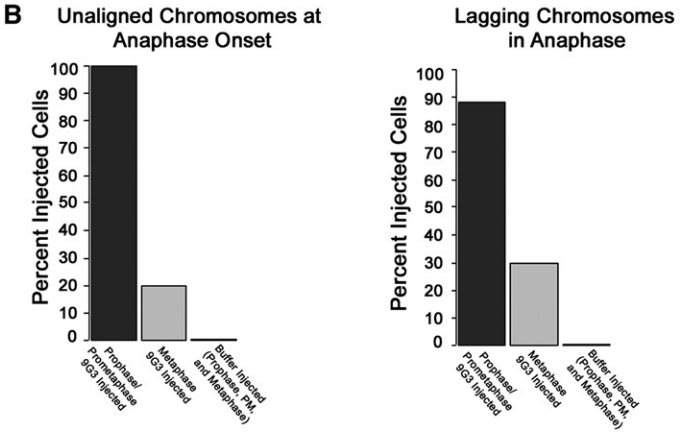

Figure 2. Mitotic Progression of Control and 9G3-Injected PtK1 Cells

(A) All cells were injected at time 0 and filmed for 2 hr. Anaphase onset is indicated as "AO." Cells shown in the top three panels were injected with 9G3 during the mitotic stage indicated. The cell shown in the bottom panel was injected in prophase with injection buffer alone. Arrows indicate lagging chromosomes in anaphase. Scale bars = 5 μm.

(B) Graphical representation of chromosome alignment errors and lagging chromosomes in buffer-injected versus 9G3-injected cells. For 9G3 injections, 17 prophase and early prometaphase cells and 10 metaphase cells were analyzed. For buffer injections, 22 prophase and prometaphase cells and 10 metaphase cells were analyzed.

The increase in centromere stretch for 9G3-injected cells suggested that kinetochores were under abnormally high tension. To further address this issue, we measured the spindle lengths in control cells and 9G3-injected cells that had a substantial number of bi-oriented chromosomes. The average metaphase spindle length for control cells was 12.8 ± 1.3 μm, while spindles in 9G3-injected cells were shorter: 9.9 μm ± 1.5 μm (Figure 3F; t test p value < 0.001). Spindle lengths were obtained by measuring the distance between the focused minus ends of

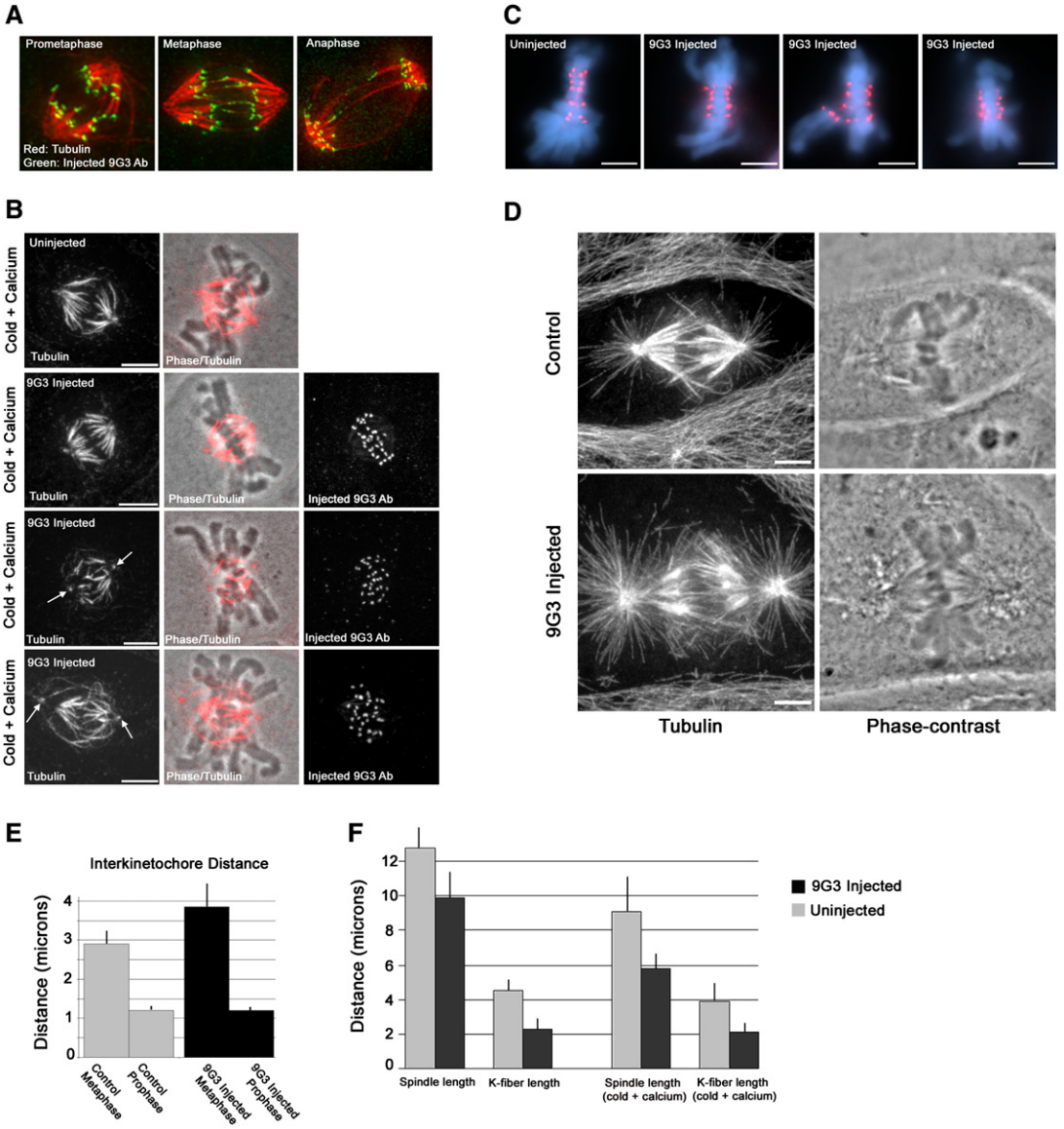

Figure 3. kMT Attachment and Spindle Structure Analysis in 9G3-Injected Cells

(A) Early to late prometaphase PtK1 cells were injected with 9G3 and fixed 20–60 min later. Immunofluorescent images were deconvolved to demonstrate that all kinetochores were attached to a bundle of MTs and merotelic attachments are prevalent.

(B) Uninjected (first row) or 9G3-injected cells (bottom 3 rows) were lysed and incubated for 90 min in ice-cold calcium buffer. Kinetochores in both uninjected and 9G3-injected cells retained robust kinetochore fibers. 9G3-injected cells exhibited varying degrees of disorganization. Centrosomes separated from minus ends of kinetochore fibers are indicated (arrows).

(C) Uninjected and 9G3-injected cells were stained with CREST serum and interkinetochore distances were analyzed.

(D) An uninjected (top) and 9G3-injected cell (bottom) were fixed in glutaraldehyde to preserve MT structure. The minus ends of the kinetochore fibers are pulled away from the aster-centers in the 9G3-injected cell.

(E) Quantification of interkinetochore distances. n values are in parentheses: control metaphase (100 kinetochore pairs/12 cells); 9G3-injected metaphase (150 kinetochore pairs/17 cells); control and 9G3-injected prophase (18 kinetochore pairs/3 cells).

(F) Quantification of spindle and kinetochore fiber lengths. Spindle lengths were measured from the minus ends of the spindle MTs, not from aster-center to aster-center. The following numbers of spindles were measured for spindle length determination: control: 12, 9G3-injected: 17, control cold-treated: 8, 9G3-injected cold-treated: 15. The following numbers of kinetochore fibers from the indicated number of cells were measured: control: 130 fibers/12 cells, 9G3-injected: 145 fibers/15 cells, control cold-treated: 90 fibers/8 cells, 9G3-injected cold-treated: 130 fibers/14 cells. Data in (E) and (F) are represented as average ± standard deviation. Scale bars in all panels = 5 μm.

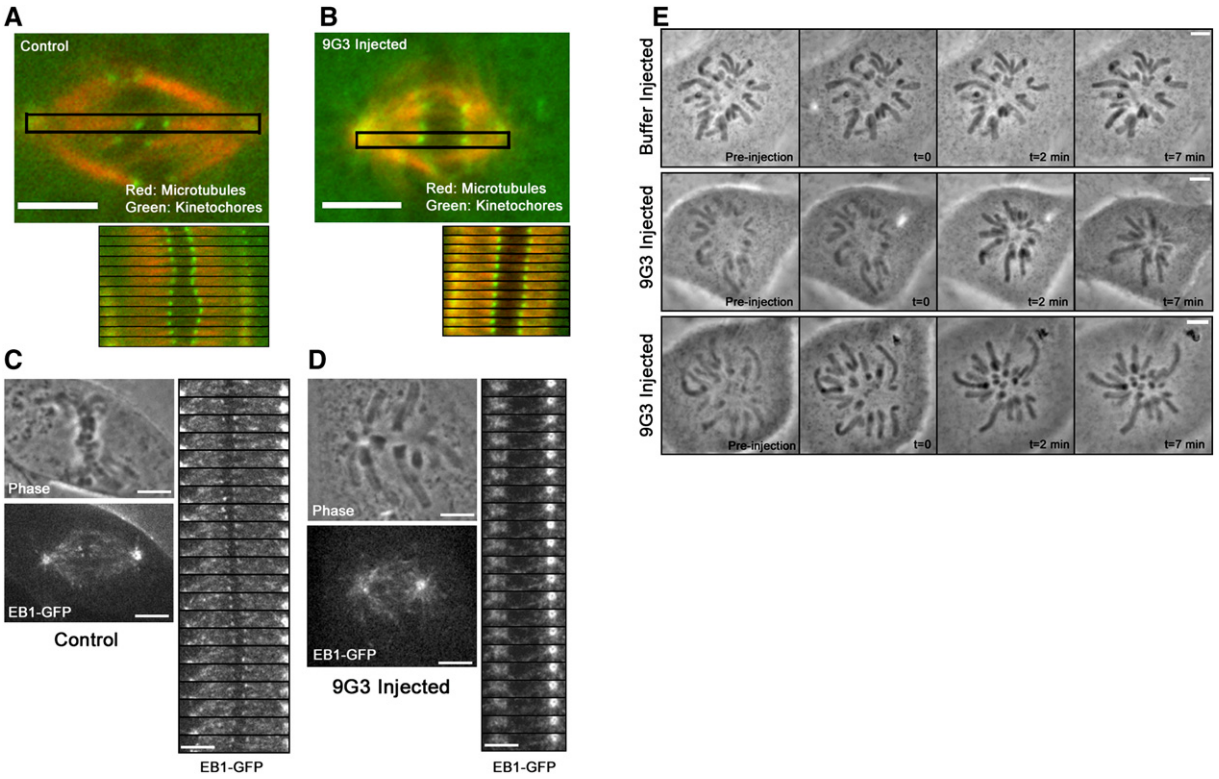

Figure 4. Loss of Kinetochore Oscillations and Plus-End MT Polymerization in Hec1 9G3-Injected Cells

(A and B) Kinetochore behavior was analyzed by live-cell fluorescence timelapse imaging. Cells were injected with rhodamine-labeled tubulin and Alexa 488-conjugated CENP-F antibodies (A), or additionally with 9G3 (B). Images were acquired every 15 s. Selected planes are shown from the timelapse sequences (A and B, top). Selected kinetochore pairs are boxed and a time series of 12 images for each pair is shown below (A and B, bottom). Kinetochores from the control cell exhibited oscillatory behavior and periods of stretching and relaxation (example in A, bottom), whereas kinetochores from the 9G3-injected cell did not oscillate (example in B, bottom).

(C and D) EB1-GFP-expressing PtK1 cells were injected with Texas Red dextran alone (C) or in combination with 9G3 (D). Images were acquired every 10 s. A region containing a kinetochore pair and the spindle poles was extracted from the timelapse sequence and shown to the right. The bright spots in extracted images are spindle poles.

(E) A buffer-injected monopolar cell exhibits chromosome oscillations toward and away from the pole both prior to and after injection (top panel). In cells injected with 9G3, chromosomes stopped oscillating and moved poleward after injection (middle and bottom panels). In all panels, scale bars = 5 μm.

the spindle MTs rather than the distance between each aster-center. This distinction is noteworthy because in many 9G3-injected cells, asters remained anchored near the cell peripheries (as in control cells), but the minus ends of the kinetochore fibers were moved away from their normal position at the edge of the centrosome (Figure 3D). This produced a large gap between the minus ends of the kinetochore fibers and each aster-center in these cells. Individual kinetochore fibers were measured and, indeed, were significantly shorter in 9G3-injected cells than in control cells (Figure 3F; t test p value < 0.001).The variation in spindle structure was likely due to individual cells' ability to remain adherent to the coverslip during mitosis. Minus ends of kMTs were displaced from aster-centers by large distances in cells that remained strongly adherent; cells that rounded up exhibited both kMT shortening and a decrease in aster-center to aster-center distance.

The N Terminus of Hec1 Specifically Regulates MT Plus-End Polymerization and Depolymerization at Kinetochores

The unexpected increase in centromere stretch and decrease in kMT length suggested that normal plus-end MT polymerization and depolymerization at the kinetochore were altered in 9G3-injected cells. We analyzed oscillations of sister kinetochore pairs, which depend on the dynamic instability of kMT plus ends (Tirnauer et al., 2002). Metaphase PtK1 cells injected with rhodamine-labeled tubulin to label MTs and a nonperturbing Alexa 488-labeled CENP-F antibody to mark kinetochores exhibited normal bi-directional kinetochore oscillations (Cimini et al., 2004; Cameron et al., 2006; Movie S1; Figure 4A). In contrast, cells injected with 9G3 contained no kinetochore pairs that exhibited any oscillatory movements (Movie S2; Figure 4B). Both merotelic and nonmerotelic kinetochores failed to oscillate. The MT tip-tracking protein

EB1 normally localizes to the polymerizing plus ends of non-kMTs and kMTs during oscillations away from the pole (Tirnauer et al., 2002). EB1 failed to persistently localize to kinetochores in 9G3-injected PtK1 cells (Figure 4C; Movie S3). However, EB1 localized to growing plus ends of non-kMTs in 9G3-injected cells identically to those in control cells, indicating that 9G3 specifically suppresses dynamics at the plus ends of kMTs.

We next determined the effect of 9G3 injection on chromosome movements in cells with monopolar spindles, in which chromosomes are either mono-oriented (only one sister kinetochore attached to the single pole) or syntelically oriented (both sisters attached to the pole) (Kapoor et al., 2000). PtK1 cells with monopolar spindles (generated by addition of 200 μM monastrol; Mayer et al.,1999; Kapoor et al., 2000), were injected with buffer alone or 9G3 and imaged by timelapse phase-contrast microscopy. Chromosomes in monopolar cells injected with buffer alone exhibited normal oscillations prior to and after injection (Figure 4E, top panel and Movie S5). In contrast, chromosomes in monopolar cells injected with 9G3 did not exhibit normal oscillations after injection. Instead, chromosomes moved poleward to an equilibrium position close to the pole (Figure 4E, middle and bottom and Movie S6). The rate of chromosome oscillations in buffer-injected cells either toward or away from the pole was 1.8 μm/min. Immediately after 9G3 injection, for ~1 min, the rate of chromosome movement poleward was 1.2 μm/min. The remainder of the poleward movement occurred at an average rate of 0.39 μm/min, which is similar to the rate of poleward flux in PtK1 monopolar spindles, 0.45 μm/min (Cameron et al., 2006). These results argue that 9G3 binding to the Hec1 N terminus initially inhibits polymerization and subsequently inhibits depolymerization of plus ends of kMTs, resulting in kinetochores immobilized on the MT lattice.

All chromosomes in 9G3-injected monopolar cells moved poleward after injection, suggesting that the MT flux machinery within the spindle remained functional after 9G3 injection and continued to produce MT depolymerization at the minus ends of kMTs. A MT motor protein that has been implicated in contributing to minus-end depolymerization activity is Kif2a, a KinI class 13 kinesin, which localizes to spindle poles (and to a lesser degree, centromeres) in tissue culture cells (Rogers et al., 2004; Ganem and Compton, 2004; Gaetz and Kapoor, 2004). In 9G3-injected cells, Kif2a remained strongly localized to the minus ends of kinetochore fibers and throughout the gap that formed between the aster-centers and the spindle MT minus ends (Figure S4). These results indicate that 9G3 injection prevents plus-end MT dynamics at the kinetochore but does not inhibit minus-end depolymerization.

Functional Hec1 N Terminus Is Required for Normal MT Turnover at Kinetochores

To directly measure kMT dynamics in 9G3-injected cells, we made fluorescent marks on MTs in PtK1 cells stably expressing photoactivatable (PA) GFP-tubulin (Figure 5). This method is suitable for measuring kMT dynamics, as fluorescent marks persist on the more stable kMTs, disappear more quickly from the less-stable non-kMTs, and dissipate within seconds from cytosolic tubulin by diffusion (Mitchison, 1989; Mitchison and Salmon, 1992; Zhai et al.,1995; Salic et al., 2004). The kinetics of fluorescence dissipation after photoactivation were fit well by a double exponential curve, $A_1e^{-k1t} + A_2e^{-k2t}$, where A_1 represents the percentage of less-stable MTs in the population (non-kMTs), and A_2 represents the more stable kMT population (Table S1). In prometaphase control spindles with mostly aligned chromosomes, 83% of the activated fluorescence dissipated with a $t_{1/2}$ of 18 s, while 17% had a $t_{1/2}$ of 7 min. The 18 s half-life corresponded to the turnover dynamics of non-kMTs within or surrounding the less abundant and more stable kMTs (Saxton et al., 1984; Cassimeris et al., 1990; Zhai et al., 1995). In late metaphase control spindles, the half-life of kMTs increased to 10 min, while the half-life of non-kMTs did not change. Here, 75% of the initial fluorescence within the activated mark region was due to non-kMTs. Antibody 9G3 injection decreased the fraction of dynamic non-kMTs within the kinetochore fibers to 44% but did not change their half-lives, which remained at $t_{1/2}$=18 s. The half-life of the more abundant kMTs, however, became greater than 38 min, indicating strong stabilization of attachment (Figure 5; Table S1).

We also determined the poleward flux rate relative to kinetochores by measuring the movement of fluorescent marks away from the chromosome mass. In control spindles, the activated spots on kMTs moved away from the chromosome mass at 0.6 μm/min (Figure 5A; Movie S7), confirming previous flux measurements (Mitchison, 1989). In 9G3-injected spindles, the persistent fluorescent marks of kMTs did not move poleward along the MT fiber but remained directly adjacent to the chromosomes throughout the duration of the timelapse (Figure 5; Movies S8 and S9).

Kinetochore Localization of Clasp1, Tog, and MCAK in 9G3-Injected Cells

Given the remarkable suppression of plus-end MT dynamics at kinetochores in 9G3-injected cells, we tested the ability of kinetochores to bind proteins implicated in regulation of dynamic instability. Recent evidence has indicated that the MT-binding protein Clasp1 is required for kMTs to switch to polymerization (Maiato et al., 2003). In control PtK1 cells, Clasp1 levels at kinetochores were low during prophase but accumulated throughout prometaphase to peak in metaphase, and the levels remained high during anaphase (Figure S5). Injection of 9G3 reduced Clasp1 protein levels at kinetochores of bi-oriented chromosomes by 50% compared to control metaphase levels (Figure S5). However, in PtK1 cells, this was the same level of Clasp1 found on kinetochores with no attached MTs (prophase cells or nocodazole-treated cells) and with stabilized kMTs (taxol-treated cells) (Figure S5).

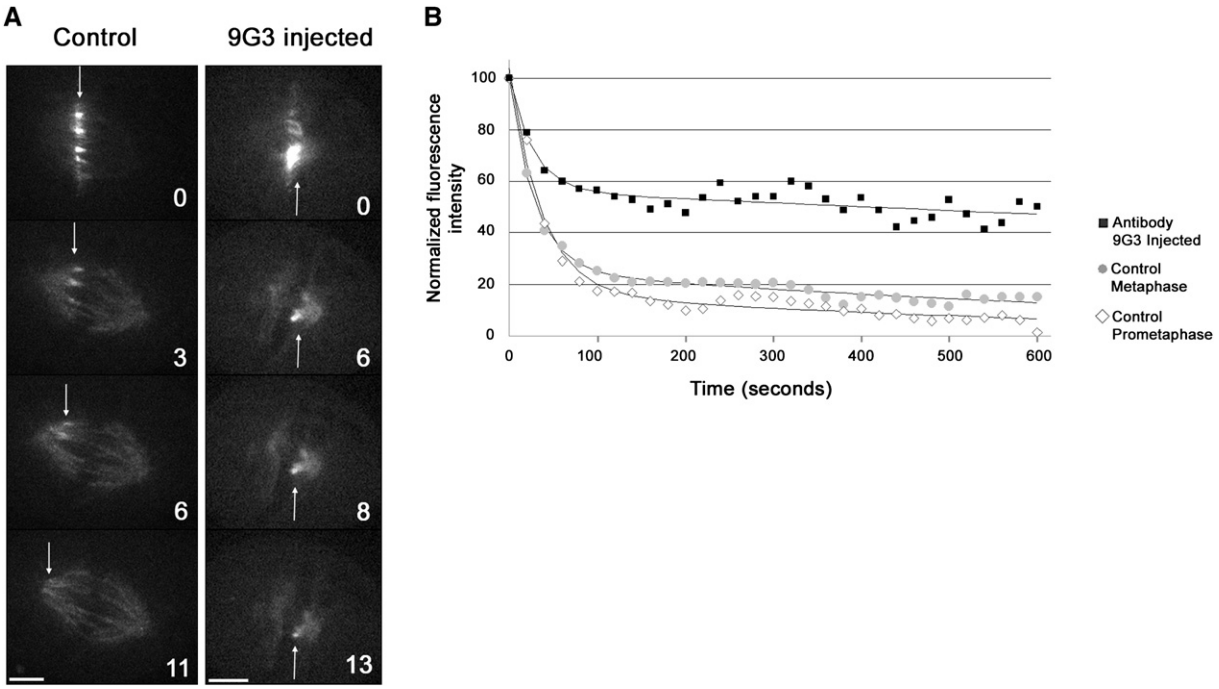

Figure 5. Effect of 9G3 Injection on kMT Stability

(A) Four frames from a timelapse of a buffer-injected (left) or 9G3-injected PtK1 cell (right) expressing PA-GFP-tubulin. Tubulin-GFP fluorescence was activated in a bar-shaped region near the chromosome mass. The arrow follows the activated region. Time is shown in min.

(B) Graph showing the decrease in fluorescence intensity of the activated regions in control metaphase cells (gray circles), control late prometaphase cells (open diamonds), and 9G3-injected late prometaphase and metaphase cells (black squares). The 9G3-injected curve was generated by averaging data at each time point from 9 cells. Late prometaphase and metaphase control curves were generated by averaging data from each time point from 7 and 12 cells, respectively. The lines through the data were obtained from nonlinear, least square fits of the data to the equation $y=A_1*\exp(-k1*t)+A_2*\exp(-k2*t)$ using SigmaPlot, as described in the text. Standard errors of regression are reported in Table S1. The data in (B) are corrected for photobleaching (see Supplemental Experimental Procedures), and the images in (A) are raw data not corrected for photobleaching, which makes a major contribution to the decrease in fluorescence at later time points.

Since accumulation of CLASP1 to high levels at kinetochores requires dynamic MTs in pre-anaphase PtK1 cells, the low levels of CLASP1 at kinetochores of 9G3-injected cells may be a consequence of inhibited MT dynamics rather than pointing to a direct role for the N terminus of Hec1 in recruiting CLASP1 to kinetochores.

We next tested the ability of kinetochores in 9G3-injected cells to bind Tog/XMAP215, a MT-binding protein that promotes polymerization (Gard and Kirschner, 1987; Vasquez et al., 1994; Charrasse et al., 1998). In both control and 9G3-injected PtK1 cells, Tog localized strongly to poles and kinetochores (Figure S6).

MCAK belongs to the class 13 kinesin family, which is a subset of kinesin-related proteins whose members induce MT depolymerization. Consistent with previous studies, control cells localized MCAK to either inner centromeres or to the kinetochore region of mitotic chromosomes (Figure S7; Andrews et al., 2004; Lan et al., 2004). MCAK localization to centromeres and kinetochores was not dependent on microtubules (data not shown). In 9G3-injected cells, fewer chromosomes exhibited centromeric MCAK and many did not accumulate detectable levels of MCAK (Figure S7), indicating that 9G3 interferes with the ability of MCAK to properly localize to mitotic chromosomes.

The N Terminus of Hec1 Is Phosphorylated at Multiple Residues by Aurora B Kinase In Vitro

We next tested the ability of human Aurora B kinase to phosphorylate the N-terminal globular domain of human Hec1. As shown in Figure 6A, an N-terminal fragment of Hec1 ($Hec1^{1–230}$, Ciferri et al., 2005) was phosphorylated in an in vitro Aurora B kinase assay, and using mass spectrometry, we mapped the following phosphorylation target sites: Ser5, Ser15, Thr49, Ser55, and Ser69. Also within the N terminus of Hec1 is an additional site, Ser44, which is predicted to be an Aurora B phosphorylation target site based on its presence within a predicted Aurora B consensus sequence (Cheeseman et al., 2002). Although we were unable to map Ser44 due to technical challenges, it is likely that this residue is phosphorylated by Aurora B kinase as well. Considering the observed defects in chromosome segregation and MT attachment in 9G3-injected cells, we tested if 9G3 had any effect on Aurora B phosphorylation of the N terminus of Hec1. Indeed, 9G3 addition decreased phosphorylation of $Hec1^{1–230}$ by 48%

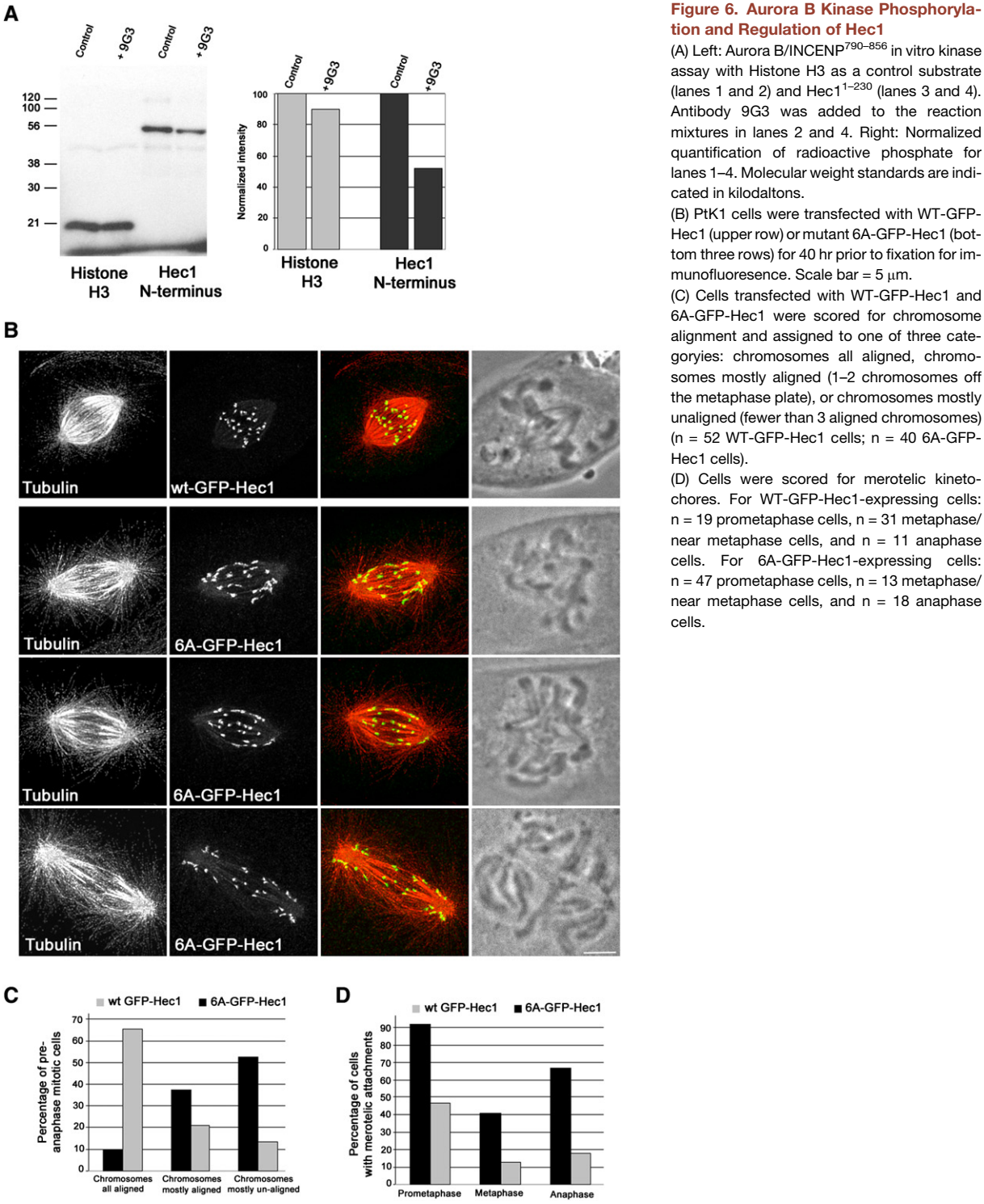

Figure 6. Aurora B Kinase Phosphorylation and Regulation of Hec1

(A) Left: Aurora B/INCENP$^{790–856}$ in vitro kinase assay with Histone H3 as a control substrate (lanes 1 and 2) and Hec1$^{1–230}$ (lanes 3 and 4). Antibody 9G3 was added to the reaction mixtures in lanes 2 and 4. Right: Normalized quantification of radioactive phosphate for lanes 1–4. Molecular weight standards are indicated in kilodaltons.

(B) PtK1 cells were transfected with WT-GFP-Hec1 (upper row) or mutant 6A-GFP-Hec1 (bottom three rows) for 40 hr prior to fixation for immunofluoresence. Scale bar = 5 μm.

(C) Cells transfected with WT-GFP-Hec1 and 6A-GFP-Hec1 were scored for chromosome alignment and assigned to one of three categoryies: chromosomes all aligned, chromosomes mostly aligned (1–2 chromosomes off the metaphase plate), or chromosomes mostly unaligned (fewer than 3 aligned chromosomes) (n = 52 WT-GFP-Hec1 cells; n = 40 6A-GFP-Hec1 cells).

(D) Cells were scored for merotelic kinetochores. For WT-GFP-Hec1-expressing cells: n = 19 prometaphase cells, n = 31 metaphase/near metaphase cells, and n = 11 anaphase cells. For 6A-GFP-Hec1-expressing cells: n = 47 prometaphase cells, n = 13 metaphase/near metaphase cells, and n = 18 anaphase cells.

(Figure 6A). Increasing the concentration of 9G3 did not decrease the level of phosphorylation further (data not shown), indicating the 9G3 concentration used was saturating.

Aurora B Phosphorylation of Hec1 N Terminus Is Essential for Normal Mitosis

We generated a mutant Hec1-GFP plasmid in which all of the five mapped target residues (Ser5, Ser15, Thr49,

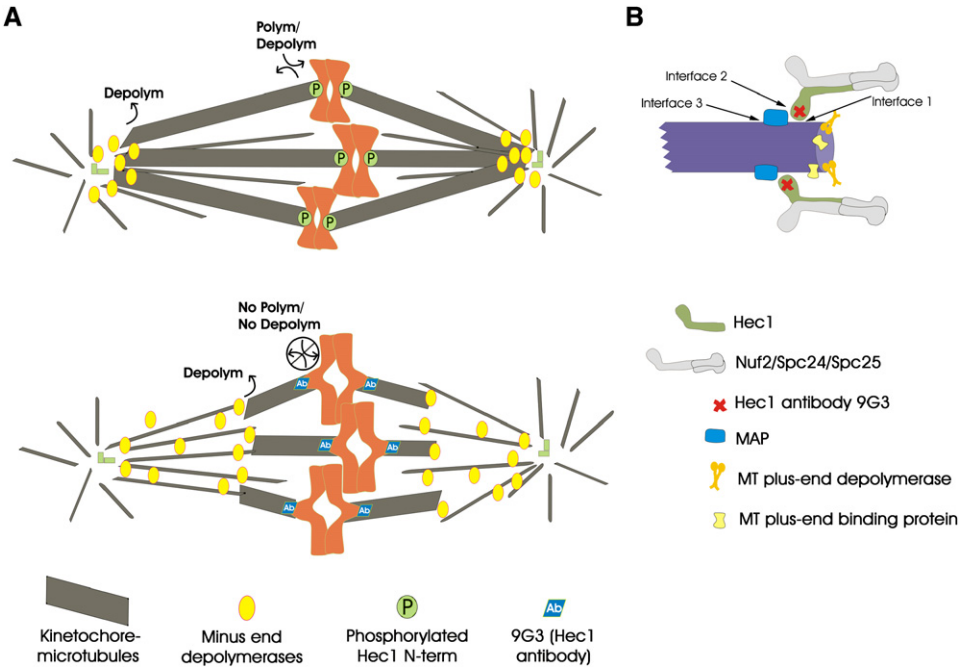

Figure 7. Model for Hec1 Regulation of kMT Dynamics and Attachment

(A) Mitotic spindle arrangement in a control cell (top) in which normal Aurora B phophorylation and dephosphorylation occur. kMT plus ends exhibit dynamic instability and undergo periods of attachment and detachment. Net polymerization at plus ends of kMTs is balanced by net depolymerization at minus ends. After addition of 9G3 (bottom), the N terminus of Hec1 can no longer be phosphorylated by Aurora B, and kMT detachment and dynamic instability are suppressed. Minus-end depolymerization is not inhibited, and active depolymerases shorten kinetochore fibers. Hyper-stretch of centromeres arises from pulling forces exerted by the centrosome-associated minus-end organizing complexes as they maintain connection with the depolymerizing minus ends of the kinetochore fibers.

(B) Regulation of kMT plus-end dynamic instability and attachment strength at three possible interfaces. Interface 1 is between the N terminus of Hec1 and the MT lattice; interface 2 is between the N terminus of Hec1 and a kinetochore-binding MAP, and interface 3 is between the MAP and the MT lattice (see text for details).

Ser55, and Ser69) and a sixth putative target site (Ser44) were mutated to alanine (6A-Hec1-GFP) to prevent Aurora B phosphorylation. Cells expressing 6A-Hec1-GFP were analyzed and compared to cells expressing a wild-type Hec1-GFP construct (WT-Hec1-GFP) by fixed cell immunofluorescence (Figure 6B). Both WT-Hec1-GFP and 6A-Hec1-GFP localized to kinetochores just prior to nuclear envelope breakdown and remained at kinetochores until late anaphase. The majority of cells (65%) expressing WT-Hec1-GFP contained all chromosomes aligned at the metaphase plate, and only 13% of the cells exhibited mostly unaligned chromosomes (the normal population of prometaphase cells) (Figure 6C). In contrast, only 10% of scored cells expressing the 6A-Hec1-GFP mutant were able to form a metaphase plate, and the majority of cells (53%) exhibited mostly unaligned chromosomes (Figure 6C). Nevertheless, these cells, like the 9G3-injected cells, proceeded into anaphase, as we did not observe an accumulation of 6A-Hec1-GFP-expressing cells in mitosis (data not shown).

The average interkinetochore distance of bi-oriented chromosomes in 6A-Hec1-GFP-expressing cells was 1.25× greater than in WT-Hec1-GFP expressing cells (t test p value < 0.001), indicating that the centromeres were hyper-stretched, as was the case in the 9G3-injected cells, albeit to a lesser degree. Cells expressing 6A-Hec1-GFP also exhibited a significantly higher incidence of merotelic attachments when compared to wt-Hec1-GFP expressing cells (Figure 6D). Our results suggest that the 6A-Hec1-GFP mutant behaves as a dominant negative in PtK1 cells, increasing the frequency of erroneous kMT attachments, inducing centromere hyper-stretch, and decreasing the fidelity of chromosome segregation.

DISCUSSION

Injection of the N-terminal Hec1 antibody produced a surprising and highly unusual mitotic phenotype (summarized in Figure 7A). Antibody 9G3 binding does not interfere with kMT formation or force generation coupled to minus-end depolymerization. However, once a MT plus end is anchored within the kMT attachment site, both attachment and plus-end assembly dynamics are stabilized. Stabilization of attachment may explain the high incidence of merotelic kinetochores and anaphase lagging chromosomes (Cimini et al., 2006) and also accounts for the loss of

kinetochore Mad2, which is normally depleted at kinetochores as they acquire a full complement of kMTs (Chen et al., 1996; Waters et al., 1998).

Our results point to a hypothesis in which Aurora B phosphorylation of the N terminus of Hec1 is involved in regulating attachment/detachment and plus-end assembly dynamics of kMTs. Ipl1p kinase has been shown to function in destabilizing kMT attachment to prevent errors in chromosome segregation in budding yeast (Tanaka et al., 2002; Cheeseman et al., 2002; Pinsky et al., 2006). Inhibition of Aurora B kinase in higher metazoa stabilizes kMT turnover in mitosis and induces errors in segregation (Maiato et al., 2004; Cimini et al., 2006). We find here that Aurora B kinase phosphorylates the Hec1 N terminus in vitro and have mapped five target sites within amino acids 1–230 of Hec1. Although we do not demonstrate that these sites are phosphorylated in vivo, at least one of the mapped sites, Ser55, has been recently identified as phosphorylated in vivo in a proteomics screen of isolated mitotic HeLa cell spindles (Nousiainen et al., 2006). Ser55 resides in a conventional Aurora B kinase consensus sequence, and this site is highly conserved in metazoa. In budding yeast, Ndc80 is phosphorylated in vivo at an Aurora B consensus target, Ser100 (Cheeseman et al., 2002). This may be the analogous site to human Ser55, but marginal sequence conservation in this region between budding yeast Ndc80 and human Hec1 prevents confirmation. Nevertheless, we did find that mutation of Aurora B target sites results in a dominant-negative phenotype similar to the 9G3 injection phenotype. The effects of expressing the 6A-Hec1-GFP mutant in PtK1 cells are somewhat less severe than the effects of 9G3 microinjection. What is not resolved is whether the dampened phenotype is a result of 9G3 disrupting additional factors at the kMT interface or is due to the fact that the mutant-expressing cells are also expressing endogenous Hec1 protein. Inhibition of Aurora B kinase by Hesperadin (Hauf et al., 2003) or ZM447439 (Cimini et al., 2006) has a more potent effect on stabilizing attachment than on blocking the oscillations of sister kinetochores on chromosomes aligned at the spindle equator. In addition, Aurora B leaves centromeres at anaphase onset (Carmena and Earnshaw, 2003) and kMTs become very stable (Zhai et al., 1995), but depolymerization and occasional polymerization occur at kinetochores at rates similar to those during oscillations before anaphase (reviewed in Maiato et al., 2004). Thus, it is likely that 9G3 not only blocks Aurora B phosphorylation of Hec1 but also disrupts additional factors that affect the kMT interface.

Interestingly, none of the five mapped sites or the 6th putative site reside within the peptide recognized by 9G3. The atomic structure of the N-terminal globular domain of Hec1 has not been solved, thus we do not know how close peptide C-2 is to the Aurora B phosphorylation sites in the native, folded protein. Antibody 9G3 may sterically inhibit Aurora B phosphorylation of the mapped residues, or amino acids 200–215 may be needed to recruit the kinase to the Hec1 N terminus. Gaining structural insight on the N terminus of Hec1 will help answer these questions.

MCAK is also phosphorylated by Aurora B kinase. Phosphorylated MCAK localizes to the inner centromere region of mitotic chromosomes, and the unphosphorylated form is routed to the outer centromere/inner kinetochore region (Lan et al., 2004; Andrews et al., 2004). This dynamic behavior of MCAK has been implicated in the correction of kMT attachment errors (reviewed in Moore and Wordeman, 2004). In 9G3-injected cells, the localization of MCAK to centromeres was perturbed. This may be a result of disrupted binding sites within the centromere after 9G3-induced hyperstretch, or alternatively, 9G3 may directly prevent proper MCAK localization. Loss of MCAK from centromeres, however, cannot account for the entire 9G3 injection phenotype, as previous studies where functional MCAK was depleted from mitotic cells did not report hyperstretched centromeres or loss of kMT dynamics (Kline-Smith et al., 2004; Moore and Wordeman, 2004; Ganem et al., 2005).

It is tempting to propose from our data that binding of 9G3 or dephosphorylation at the N terminus of Hec1 causes the Hec1 head to tightly bind to the MT lattice (interface 1 in Figure 7B). This would account for stabilization of both MT attachment and assembly dynamics within the kinetochore attachment site. In support of this, recent evidence from *C. elegans* and human cells suggests that the Ndc80 complex directly binds MTs, and this binding is regulated, in part, by Aurora B kinase (Cheeseman et al., 2006 [this issue of *Cell*]). Data from budding yeast suggest that the linkage from the Ndc80 complex to the MT lattice, rather than being direct, may be through the Dam1/DASH complex. Ipl1p phosphorylation of Ndc80 and the Dam1/DASH complex is reported to cause MT detachment from kinetochores by release of kinetochore-bound Ndc80 from the Dam1/DASH complex bound to MTs (Shang et al., 2003). When purified from budding yeast, the Dam1/DASH complex forms rings around MTs made in vitro, which can slide along the MT lattice as MTs depolymerize (Miranda et al., 2005; Westermann et al., 2005). In the "sliding ring" model, the stability of binding at the interface between the N terminus of Hec1 and the MAP (interface 2) need not affect the slippage of the MT lattice through the ring complex (interface 3, Figure 7B), which is coupled to MT polymerization and depolymerization at the kinetochore. The mammalian homolog of Dam1/DASH has not yet been found, but if a similar mechanism dynamically links MT ends to vertebrate kinetochores, our data indicate that the N terminus of Hec1 controls not only attachment to the MAP (interface 2, Figure 7B) but also slippage through the ring (interface 3, Figure 7B).

Alternatively, the binding of the MAP to the MT may be constitutively stable and would preclude a sliding ring mechanism. In this case, both MT attachment to the kinetochore and polymerization/depolymerization within the attachment site are both governed by the strength of binding between the N terminus of Hec1 and the MAP

(interface 2, Figure 7B). This model requires a high number of interface 2 binding sites within an attachment site, as many weak linkages are needed to maintain anchorage during periods of high kinetochore tension while allowing MT flux through the attachment site coupled to plus-end polymerization and depolymerization (Hill, 1985). Clearly, it will be important in the future to determine how each of the three potential interfaces in Figure 7B contribute to kMT attachment stability and plus-end assembly dynamics.

EXPERIMENTAL PROCEDURES

Hec1 Antibody Epitope Mapping

A peptide array (containing peptides of 15 amino acids in length with a 7 amino acid overlap) covering the entire human Hec1 sequence was generated (New England Peptide, Gardner, MA). Peptides were spotted on nitrocellulose and subjected to an immunoblot using the Hec1 monoclonal antibody 9G3 (Novus Biologicals, Littleton, CO, NB 100–338).

Cell Culture, Microinjections, and Drug Treatment

HeLa and Ptk1 cells were cultured as described previously (DeLuca et al., 2005; Howell et al., 2000). Antibody 9G3 was concentrated into Injection Buffer (IB: 10 mM Na_2HPO_4, pH 7.4, 100 mM KCl, and 1 mM $MgCl_2$) to a final needle concentration of 0.5–0.8 mg/ml. Injection of ~10% of the cell volume was carried out as described previously (Howell et al., 2000). IB alone or nonperturbing Alexa 488-labeled CENP-F antibodies (needle concentration = 0.75 mg/ml) were injected into mitotic cells as a control. For phase-contrast imaging, multiple cells were microinjected, and using a Ludl rotary-encoded scanning stage, a Hamamatsu Orca II camera, and MetaMorph software (Molecular Devices Corp., Sunnyvale, CA), images were acquired every 2 min for 2 hr.

Monopolar spindles were generated by incubation of PtK1 cells with 200 μM monastrol (Sigma) for 20 min. Cells were mounted in chambers with HEPES-buffered L-15 media topped with a layer of mineral oil, and images were acquired every 7 s using a 40× phase-contrast objective for 10 min. Rates of chromosome movement were measured using the "track points" function in the MetaMorph software package.

Fluorescence Imaging and Tubulin Photoactivation

For fluorescence imaging of EB1-GFP transfected cells, 25 μg/ml Texas Red dextran was included to identify injected cells. Cells were imaged using a Nikon 100× Planapochromat oil immersion lens (Garden City, NY) on a spinning disk confocal fluorescence microscope. For fluorescence imaging of MTs and kinetochores, cells were injected with rhodamine-labeled tubulin and Alexa 488-labeled CENP-F antibodies diluted into IB and imaged as described above.

Photoactivation studies were carried out as described in Cimini et al., 2006 (see Supplemental Experimental Procedures).

Immunofluorescence, Deconvolution, and Linear Protein Mapping

Primary antibodies were used at the following concentrations: Hec1 at 1:1000 (Novus Biologicals), α tubulin DM1α (Sigma) at 1:300, MCAK at 1:500 (Dr. C. Walczak, Indiana University), TOG at 1:700 (Dr. L. Cassimeris, Lehigh University), Spc24 at 1:400 (Dr. P.T. Stukenberg, University of Virginia), Kif2a at 1:500 (Dr. D.A. Compton, Dartmouth), and Clasp at 1:1000 (Dr. R. Heald, University of California, Berkeley). Immunofluorescence was carried out as described in Howell et al., 2000 (see Supplemental Experimental Procedures).

Selected images were deconvolved as described in DeLuca et al., 2005, using a Delta Vision image processing workstation (Applied Precision, Seattle, WA). The linescan function of the MetaMorph software system was used on immunofluorescent images of Spc24 and Hec1 for spatial mapping.

For cold/calcium-induced MT depolymerization experiments, cells were lysed with 0.5% Triton X-100 in PHEM buffer plus 10 mM MgATP for 5 min at 20°C. Cells were then incubated for 90 min at 4°C in a high calcium buffer (60 mM PIPES, 25 mM HEPES, 4 mM $MgCl_2$, and 10 mM $CaCl_2$ at pH 7.0).

Kinase Assays

Kinase buffers were Tris assay dilution buffer (6.7 mM Tris-HCl pH 7.5, 0.013 mM EGTA, 2 mM DTT), 1XIB, Magnesium/ATP cocktail (27.5 mM $MgCl_2$ and 183.3 μM ATP in 4 mM MOPS, pH 7.2, 9.17 mM β-glycerol phosphate, 1.83 mM EGTA, 0.37 mM sodium orthovanadate, 0.37 mM DTT). Buffer for Aurora B + $INCENP^{790–856}$ was 50 mM Tris HCl, pH 7.6, 150 mM NaCl, 1 mM DTT, 1 mM EDTA. Buffer for purified $Hec1^{1–230}$ was 300 mM KCl, 20 mM HEPES, 0.5 mM $MgCl_2$. Kinase reactions (25 μl) were prepared by diluting Aurora B (1 μg) and $INCENP^{790–856}$ (1 μg) into Tris assay dilution buffer, Magnesium/ATP cocktail, and IB. Reactions were preincubated for 10 min at 30°C to activate the Aurora B/ $INCENP^{790–856}$ complex with ATP. In other tubes, one containing Histone H3 (1 μg) or $Hec1^{1–230}$ (1 μg) with IB and the other with Histone H3 (1 μg) or $Hec1^{1–230}$ (1 μg) with 9G3 in IB, were preincubated for 10 min at 30°C. Aurora B/ $INCENP^{790–856}$ complex mixture was then added to Histone H3 or $Hec1^{1–230}$. [γ-32P]-ATP (Perkin Elmer, Wellesley, MA) in Mg/ATP buffer was added to the reactions and incubated for 20 min at 30°C. Reactions were terminated by addition of 5× Laemmli sample buffer and resolved by 10% SDS-PAGE. Radioactive phosphate incorporation into Aurora B substrates was visualized and quantified by autoradiography and phosphorimaging.

Analysis of Aurora B kinase phosphorylation of $Hec1^{1–230}$ was performed on tryptically digested peptides separated by reversed-phase chromatography by tandem mass spectrometry (MS/MS). Mass spectra were aquired on a Q-TRAP (Applied Biosystems), a hybrid combining quadrupole and ion-trap mass analyzers, which was operated in "enhanced" scan mode for increased sensitivity suitable for the low-level phosphorylation analysis (Le Blanc et al., 2003). The resulting spectra were searched against the Hec1 sequence, with potential S/T phosphorylation, using an in-house version of the Mascot (Matrix Science Limited) search engine (Perkins et al., 1999). Mass spectrometry data were acquired at the UNC-Duke Proteomics Center.

GFP-Hec1 Mutation and Expression

Targeted alanine PCR-mediated mutagenesis was carried out using QuikChange Multi and XL-II Site-Directed Mutagenesis kits (Stratagene, La Jolla, CA) in a pEGFP-Hec1 vector. WT-GFP-Hec1 or 6A-GFP-Hec1 were transfected into PtK1 cells using Fugene 6 (Roche, Basel, Switzerland). Cells were immunostained with tubulin DM1α antibodies and anti-GFP antibodies (Sigma).

Supplemental Data

Supplemental Data include experimental procedures, seven figures, one table, and nine movies and can be found with this article online at http://www.cell.com/cgi/content/full/127/5/969/DC1/.

ACKNOWLEDGMENTS

We thank Dr. A. Khodjakov for PA-GFP-tubulin-expressing PtK1 cells and Dr. J. Tirnauer for GFP-EB1-expressing PtK1 cells. We thank the following for antibodies: Dr. P.T. Stukenberg, Dr. L. Cassimeris, Dr. C. Walczak, Dr. D. Compton, Dr. D. Cleveland, and Dr. R. Heald. We thank Jessica Polka, Ryan O'Quinn, and Drs. Chad Pearson, Kerry Bloom, and Ajit Joglekar for critical reading of the manuscript and Dr. Iain Cheeseman for insight on the project. This work was supported by NIH GM24364 to E.D.S., NIH GM66588 to J.G.D., NIH GM67370 to W.E.G., and HFSP RGP29/2003 to A.M. and E.D.S. This work was supported by EU Framework Program FP6 grants Mitocheck and 3D-Repertoire (to A.M.).

Received: January 9, 2006
Revised: May 19, 2006
Accepted: September 5, 2006
Published: November 30, 2006

REFERENCES

Andrews, P.D., Ovechkina, Y., Morrice, N., Wagenbach, M., Duncan, K., Wordeman, L., and Swedlow, J.R. (2004). Aurora B regulates MCAK at the mitotic centromere. Dev. Cell *6*, 253–268.

Brinkley, B.R., and Cartwright, J., Jr. (1975). Cold-labile and cold-stable microtubules in the mitotic spindle of mammalian cells. Ann. N Y Acad. Sci. *253*, 428–439.

Cameron, L.A., Yang, G., Cimini, D., Canman, J.C., Kisurina-Evgenieva, O., Khodjakov, A., Danuser, G., and Salmon, E.D. (2006). Kinesin 5-independent poleward flux of kinetochore microtubules in PtK1 cells. J. Cell Biol. *173*, 173–179.

Carmena, M., and Earnshaw, W.C. (2003). The cellular geography of aurora kinases. Nat. Rev. Mol. Cell Biol. *4*, 842–854.

Cassimeris, L., Rieder, C.L., Rupp, G., and Salmon, E.D. (1990). Stability of microtubule attachment to metaphase kinetochores in PtK1 cells. J. Cell Sci. *96*, 9–15.

Charrasse, S., Schroeder, M., Gauthier-Rouviere, C., Ango, F., Cassimeris, L., Gard, D.L., and Larroque, C. (1998). The TOGp protein is a new human microtubule-associated protein homologous to the Xenopus XMAP215. J. Cell Sci. *111*, 1371–1383.

Cheeseman, I.M., Brew, C., Wolyniak, M., Desai, A., Anderson, S., Muster, N., Yates, J.R., Huffaker, T.C., Drubin, D.G., and Barnes, G. (2001). Implication of a novel multiprotein Dam1p complex in outer kinetochore function. J. Cell Biol. *155*, 1137–1145.

Cheeseman, I.M., Anderson, S., Jwa, M., Green, E.M., Kang, J., Yates, J.R., 3rd, Chan, C.S., Drubin, D.G., and Barnes, G. (2002). Phosphoregulation of kinetochore microtubule attachments by the Aurora kinase Ipl1p. Cell *111*, 163–172.

Cheeseman, I.M., Chapple, J.S., Wilson-Kubalek, E.M., and Desai, A. (2006). The conserved KMN network constitutes the core microtubule binding site of the kinetochore. Cell *127*, this issue, 983–997.

Chen, R.H., Waters, J.C., Salmon, E.D., and Murray, A.W. (1996). Association of spindle assembly checkpoint component XMAD2 with unattached kinetochores. Science *274*, 242–246.

Chen, Y., Riley, D.J., Chen, P.L., and Lee, W.H. (1997). HEC, a novel nuclear protein rich in leucine heptad repeats specifically involved in mitosis. Mol. Cell. Biol. *17*, 6049–6056.

Ciferri, C., De Luca, J., Monzani, S., Ferrari, K.J., Ristic, D., Wyman, C., Stark, H., Kilmartin, J., Salmon, E.D., and Musacchio, A. (2005). Architecture of the human Ndc80-Hec1 complex, a critical constituent of the outer kinetochore. J. Biol. Chem. *280*, 29088–29095.

Cimini, D., Howell, B., Maddox, P., Khodjakov, A., Degrassi, F., and Salmon, E.D. (2001). Merotelic kinetochore orientation is a major mechanism of aneuploidy in mitotic mammalian tissue cells. J. Cell Biol. *153*, 517–527.

Cimini, D., Moree, B., Canman, J.C., and Salmon, E.D. (2003). Merotelic kinetochore orientation occurs frequently during early mitosis in mammalian tissue cells and error correction is achieved by two different mechanisms. J. Cell Sci. *116*, 4213–4225.

Cimini, D., Cameron, L.A., and Salmon, E.D. (2004). Anaphase spindle mechanics prevent mis-segregation of merotelically oriented chromosomes. Curr. Biol. *14*, 2149–2155.

Cimini, D., Wan, X., Hirel, C., and Salmon, E.D. (2006). Aurora kinase promotes turnover of kinetochore microtubules to reduce chromosome segregation errors due to merotelic kinetochore orientation. Curr. Biol. *16*, 1711–1718.

DeLuca, J.G., Dong, Y., Hergert, P., Strauss, J., Hickey, J.M., Salmon, E.D., and McEwen, B.F. (2005). Hec1 and Nuf2 are core components of the kinetochore outer plate essential for organizing MT attachment sites. Mol. Biol. Cell *16*, 519–531.

Gaetz, J., and Kapoor, T.M. (2004). Dynein/dynactin regulate metaphase spindle length by targeting depolymerizing activities to spindle poles. J. Cell Biol. *166*, 465–471.

Ganem, N.J., and Compton, D.A. (2004). The KinI kinesin Kif2a is required for bipolar spindle assembly through a functional relationship with MCAK. J. Cell Biol. *166*, 473–478.

Ganem, N.J., Upton, K., and Compton, D.A. (2005). Efficient mitosis in human cells lacking poleward microtubule flux. Curr. Biol. *15*, 1827–1832.

Gard, D.L., and Kirschner, M.W. (1987). A microtubule-associated protein from Xenopus eggs that specifically promotes assembly at the plus-end. J. Cell Biol. *105*, 2203–2215.

Hauf, S., Cole, R.W., LaTerra, S., Zimmer, C., Schnapp, G., Walter, R., Heckel, A., van Meel, J., Rieder, C.L., and Peters, J.M. (2003). The small molecule Hesperadin reveals a role for Aurora B in correcting kinetochore-microtubule attachment and in maintaining the spindle assembly checkpoint. J. Cell Biol. *161*, 281–294.

Hill, T.L. (1985). Theoretical problems related to the attachment of microtubules to kinetochores. Proc. Natl. Acad. Sci. USA *82*, 4404–4408.

Howell, B.J., Hoffman, D.B., Fang, G., Murray, A.W., and Salmon, E.D. (2000). Visualization of Mad2 dynamics at kinetochores, along spindle fibers, and at spindle poles in living cells. J. Cell Biol. *150*, 1233–1250.

Kapoor, T.M., Mayer, T.U., Coughlin, M.L., and Mitchison, T.J. (2000). Probing spindle assembly mechanisms with monastrol, a small molecule inhibitor of the mitotic kinesin, Eg5. J. Cell Biol. *150*, 975–988.

Kline-Smith, S.L., Khodjakov, A., Hergert, P., and Walczak, C.E. (2004). Depletion of centromeric MCAK leads to chromosome congression and segregation defects due to improper kinetochore attachments. Mol. Biol. Cell *15*, 1146–1159.

Lan, W., Zhang, X., Kline-Smith, S.L., Rosasco, S.E., Barrett-Wilt, G.A., Shabanowitz, J., Hunt, D.F., Walczak, C.E., and Stukenberg, P.T. (2004). Aurora B phosphorylates centromeric MCAK and regulates its localization and MT depolymerization activity. Curr. Biol. *14*, 273–286.

Le Blanc, J.C., Hager, J.W., Ilisiu, A.M., Hunter, C., Zhong, F., and Chu, I. (2003). Unique scanning capabilities of a new hybrid linear ion trap mass spectrometer (Q TRAP) used for high sensitivity proteomics applications. Proteomics *3*, 859–869.

Maiato, H., Fairley, E.A.L., Rieder, C.L., Swedlow, J.R., Sunkel, C.E., and Earnshaw, W.C. (2003). Human CLASP1 is an outer kinetochore component that regulates spindle microtubule dynamics. Cell *113*, 891–904.

Maiato, H., DeLuca, J., Salmon, E.D., and Earnshaw, W.C. (2004). The dynamic kinetochore-microtubule interface. J. Cell Sci. *117*, 5461–5477.

Mao, Y., Abrieu, A., and Cleveland, D.W. (2003). Activating and silencing the mitotic checkpoint through CENP-E-dependent activation/inactivation of BubR1. Cell *114*, 87–98.

Mayer, T.U., Kapoor, T.M., Haggarty, S.J., King, R.W., Schreiber, S.L., and Mitchison, T.J. (1999). Small molecule inhibitor of mitotic spindle bipolarity identified in a phenotype-based screen. Science *286*, 971–974.

McCleland, M.L., Kallio, M.J., Barrett-Wilt, G.A., Kestner, C.A., Shabanowitz, J., Hunt, D.F., Gorbsky, G.J., and Stukenberg, P.T. (2004). The vertebrate Ndc80 complex contains Spc24 and Spc25 homologs, which are required to establish and maintain kinetochore-microtubule attachment. Curr. Biol. *14*, 131–137.

Miranda, J.J., De Wulf, P., Sorger, P.K., and Harrison, S.C. (2005). The yeast DASH complex forms closed rings on microtubules. Nat. Struct. Mol. Biol. *12*, 138–143.

Mitchison, T.J. (1989). Polewards microtubule flux in the mitotic spindle: evidence from photoactivation of fluorescence. J. Cell Biol. *109*, 637–652.

Mitchison, T.J., and Salmon, E.D. (1992). Poleward kinetochore fiber movement occurs during both metaphase and anaphase-A in newt lung cell mitosis. J. Cell Biol. *119*, 569–582.

Moore, A., and Wordeman, L. (2004). The mechanism, function and regulation of depolymerizing kinesins during mitosis. Trends Cell Biol. *14*, 537–546.

Nousiainen, M., Sillje, H.H., Sauer, G., Nigg, E.A., and Korner, R. (2006). Phosphoproteome analysis of the human mitotic spindle. Proc. Natl. Acad. Sci. USA *103*, 5391–5396.

Perkins, D.N., Pappin, D.J., Creasy, D.M., and Cottrell, J.S. (1999). Probability-based protein identification by searching sequence databases using mass spectrometry data. Electrophoresis *20*, 3551–3567.

Pinsky, B.A., Kung, C., Shokat, K.M., and Biggins, S. (2006). The Ipl1-Aurora protein kinase activates the spindle checkpoint by creating unattached kinetochores. Nat. Cell Biol. *8*, 78–83.

Rogers, G.C., Rogers, S.L., Schwimmer, T.A., Ems-McClung, S.C., Walczak, C.E., Vale, R.D., Scholey, J.M., and Sharp, D.J. (2004). Two mitotic kinesins cooperate to drive sister chromatid separation during anaphase. Nature *427*, 364–370.

Salic, A., Waters, J.C., and Mitchison, T.J. (2004). Vertebrate shugoshin links sister centromere cohesion and kinetochore microtubule stability in mitosis. Cell *118*, 567–578.

Saxton, W.M., Stemple, D.L., Leslie, R.J., Salmon, E.D., Zavortink, M., and McIntosh, J.R. (1984). Tubulin dynamics in cultured mammalian cells. J. Cell Biol. *99*, 2175–2186.

Shang, C., Hazbun, T.R., Cheeseman, I.M., Aranda, J., Fields, S., Drubin, D.G., and Barnes, G. (2003). Kinetochore protein interactions and their regulation by the Aurora kinase Ipl1p. Mol. Biol. Cell *14*, 3342–3355.

Tanaka, T.U., Rachidi, N., Janke, C., Pereira, G., Galova, M., Schiebel, E., Stark, M.J., and Nasmyth, K. (2002). Evidence that the Ipl1-Sli15 (Aurora kinase-INCENP) complex promotes chromosome bi-orientation by altering kinetochore-spindle pole connections. Cell *108*, 317–329.

Tien, A.C., Lin, M.H., Su, L.J., Hong, Y.R., Cheng, T.S., Lee, Y.C., Lin, W.J., Still, I.H., and Huang, C.Y. (2004). Identification of the substrates and interaction proteins of aurora kinases from a protein-protein interaction model. Mol. Cell. Proteomics *3*, 93–104.

Tirnauer, J.T., Salmon, E.D., and Mitchison, T.J. (2004). Microtubule plus-end dynamics in Xenopus egg extract spindles. Mol. Biol. Cell *15*, 1776–1784.

Tirnauer, J.S., Canman, J.C., Salmon, E.D., and Mitchison, T.J. (2002). EB1 targets to kinetochores with attached, polymerizing microtubules. Mol. Biol. Cell *13*, 4308–4316.

Vasquez, R.J., Gard, D.L., and Cassimeris, L. (1994). XMAP from Xenopus eggs promotes rapid plus end assembly of microtubules and rapid microtubule polymer turnover. J. Cell Biol. *127*, 985–993.

Waters, J.C., Chen, R.H., Murray, A.W., and Salmon, E.D. (1998). Localization of Mad2 to kinetochores depends on microtubule attachment, not tension. J. Cell Biol. *141*, 1181–1191.

Wei, R.R., Sorger, P.K., and Harrison, S.C. (2005). Molecular organization of the Ndc80 complex, an essential kinetochore component. Proc. Natl. Acad. Sci. USA *102*, 5363–5367.

Weisenberg, R.C., and Deery, W.J. (1981). The mechanism of calcium-induced microtubule disassembly. Biochem. Biophys. Res. Commun. *102*, 924–931.

Westermann, S., Avila-Sakar, A., Wang, H.W., Niederstrasser, H., Wong, J., Drubin, D.G., Nogales, E., and Barnes, G. (2005). Formation of a dynamic kinetochore-microtubule interface through assembly of the Dam1 ring complex. Mol. Cell *17*, 277–290.

Zhai, Y., Kronebusch, P.J., and Borisy, G.G. (1995). Kinetochore microtubule dynamics and the metaphase-anaphase transition. J. Cell Biol. *131*, 721–734.